

# Impact Research of High Photovoltaics Penetration Using High Resolution Resource Assessment with Sky Imager and Power System Simulation

Dung (Andu) Nguyen, Pablo Ubiratan, Maxim Velay, Ryan Hanna, Jan Kleissl, Jens Schoene, Vadim Zheglov, Ben Kurtz, Bill Torre, Vahid Disfani

**Abstract**— Some of the adverse impacts of high photovoltaics (PV) penetration on the power grid are an increasing number of tap operations, over-voltages, and large and frequent voltage fluctuations and PV power ramps. However, the inability to create realistic PV input profiles with high spatial and temporal resolution make the results of prior studies questionable. This report proposes a unique method to realistically investigate these impacts and assess a feeder's hosting capacity using (1) high resolution PV generation profiles with sky imagers, (2) quasi-steady state distribution system simulation, and (3) five distribution models created from data provided by a Californian utility. Solar penetration levels, defined as peak PV output divided by peak load demand, are varied from 0% to 200%. The distribution system state was simulated over 3 contiguous months in December 2014 – March 2015. The following conclusions were derived: (1) the impacts of high PV penetration depend strongly on the feeder topology and characteristics; (2) the use of a single PV generation profile overestimates the number of tap operations up to 70% due to an overestimation of power ramp rates and magnitudes. Thus multiple realistic profiles should be used for distribution system analyses.

## I. INTRODUCTION

Addressing the intermittent disturbances in solar power output caused by clouds to ensure that the grid is not unduly disturbed and that power quality is maintained is a key element of the technical challenge to the grid integration of high solar PV penetration. Several recent studies [1], [2] have reviewed the potential issues with high PV penetration. Although there is significant interest in the potential issues of high PV penetration, investigations with high resolution and realistic generation profiles of PV systems are lacking. While most PV system impact studies either use the same solar generation profile for all PV systems and/or low resolution PV profiles [3]-[5], short term PV ramp rates have been shown to become uncorrelated over distances as short as a few 100 m [6]. Therefore, applying just a single or a few PV profiles to all systems on the feeder may lead to unrealistic results due to the distributed nature of the generation and the resulting geographic diversity effect. This would lead to erroneous assessments of wear-and-tear on voltage regulation equipment caused by solar power variability.

In this report, we propose a unique approach to overcome this limitation using granular solar resource modeling with a sky imager to provide PV generation profiles with high temporal and spatial resolution. The profiles are applied to realistic and topology-diverse distribution models that are modeled in quasi-steady state with OpenDSS [18] to examine distribution feeder impacts at various PV penetration levels. The novel approach presented herein provides realistic PV power output at high temporal and spatial resolution and thus considers spatial variability of solar generation in a realistic manner.

## II. FEEDER MODELS AND DATA

### A. Five Distribution Feeder Models

System information for five distribution feeders with high PV penetration were provided by the host utility in SynerGEE and used to create equivalent distribution models in OpenDSS. Short circuit currents and power flow results from SynerGEE simulations were used to validate our models. Table I and Figures 1-5 summarize the characteristics of these feeders. Feeders A, D, and E are in rural areas. Feeders B and C are in urban areas. Feeder A has two large PV systems at the end of the circuit, the largest load demand and a long feeder length. This leads to large drop in voltage along the feeder (Figure 2) when load demand is high and no PV power output present. The large voltage drop in this case violates the ANSI lower voltage bound of 0.95 p.u. However, this would not occur in practice since it is unlikely that all the loads demand maximum power simultaneously. The daily load demand is usually between 30% and 70% of the maximum load. These numbers are even lower when we consider the

increasing amount of distributed generation. Feeder A presents a worst case scenario for solar power integration given the combination of long lines, thin wires, and the large PV system being situated at the end of the feeder.

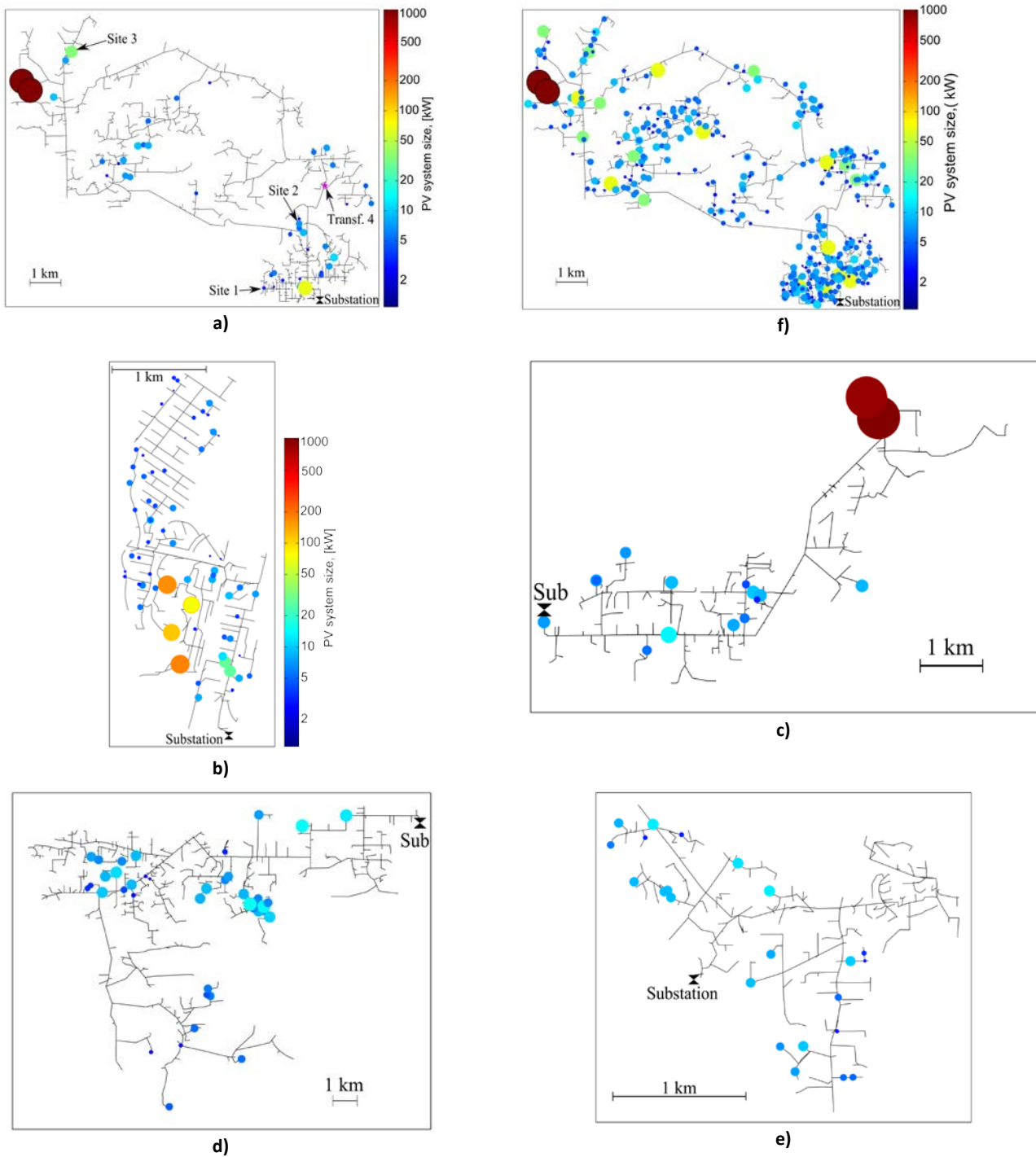


**Figure 1. Plan view of the feeders studied with location and size of actual PV systems as of 2012. The size (rated AC output power) of the PV sites can be gleaned from (1) the color, based on the logarithmic color scale in the figure, and (2) the size of the circle with the area of the circle being proportional to the log of the rated output power. a) Feeder A, b) feeder B, c) feeder C, d) feeder D, e) feeder E, f) Feeder A with additional PV systems to vary the penetration level.**

All graphs show the solar systems as of 2012. Only for feeder A the top row shows feeder A with 44 original PV systems and 387 additional virtual distributed PV systems created for simulations with high PV penetration.

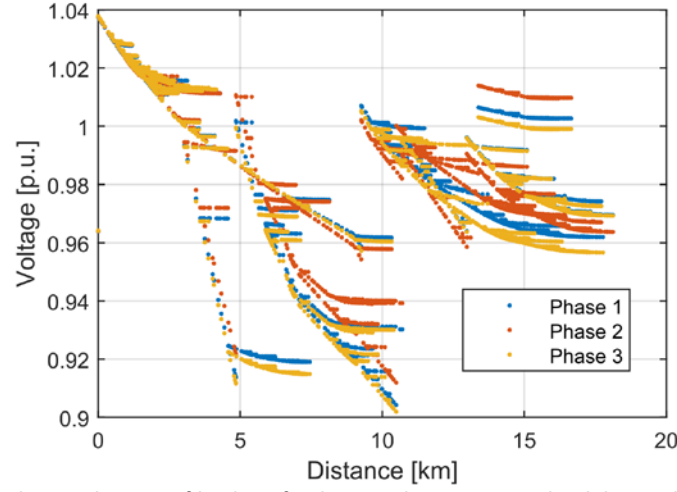


Figure 2. Normalized balanced 3-phase voltage profile along feeder A with 11 MW max load demand and no PV output. The voltage level drops to as low as 0.90 p.u. in the middle of the feeder even when the substation voltage level is raised to 1.03 p.u.

Table I: Characteristics of distribution feeders.

Circuit	A	B	C	D	E
Feeder length (km)	177.8	39.6	34.9	51.5	115.7
No. of Loads	1733	584	471	468	1178
Total peak load (MW)	11.1	8.3	4.8	3.7	5.9
No. of Capacitor banks	5	0	0	0	0
No. of Transformers & VRs	7	1	2	2	2
No. of PV systems (in 2012)	45	85	28	19	43
No. of PV systems (simulated)	432	340	364	104	387
Total rated PV capacity (MW <sub>AC</sub> in 2012)	2.3	1.3	0.2	2.1	0.3
Large PV systems (#>0.5MW)	2	0	0	2	0
**Large PV systems (#>0.5MW)	2	0	0	2	0
PV penetration in 2012	21%	15%	4%	58%	5%
Total rated PV capacity (MW <sub>AC</sub> ) and PV penetration required to flatten daytime load in 2015	5.9 53%	6.0 72%	4.3 90%	2.9 78%	10.6 180%

### B. Variable PV Penetration

As of 2012, based on California Solar Initiative incentive data the feeders were populated with PV systems. Fig. 1 illustrates feeder A with 45 existing PV systems. The locations of the mapped PV sites are depicted by circles. Feeder A has two large 1 MW PV plants and Feeder D has a 1.13 MW PV plant. Feeder B has 8 commercial-sized PV systems ranging from 70 kW to 174 kW, totaling 909 kW. The remaining PV systems are residential with an average size of 6 kW. Table I provides some information on the existing PV systems on these feeders. The locations and sizes of PV systems are shown in Figs. 1-5.

The PV penetration levels of the feeders are different and range from 4% to 57.7%. PV penetration level is calculated as:

$$p = \frac{P_{\text{rated\_pv\_peak}}}{P_{\text{rated\_load\_peak}}} \quad (1),$$

where  $P_{\text{rated\_pv\_peak}}$  and  $P_{\text{rated\_load\_peak}}$  are the rated total AC (inverter) power of the PV systems and rated peak total consumption of the loads in the feeder, respectively. Other definitions for PV penetration level that could be used are:

$$p_{\text{daily}} = \frac{P_{\text{max\_daily\_pv\_production}}}{P_{\text{max\_daily\_load\_peak}}} \quad (2),$$

and

$$p_{\text{energy\_daily}} = \frac{E_{\text{total\_daily\_pv\_production}}}{E_{\text{total\_daily\_load\_consumption}}} \quad (3),$$

where  $P_{\text{max\_daily\_pv\_production}}$  and  $P_{\text{max\_daily\_load\_peak}}$  are maximum daily PV power production and maximum daily load power consumption; while  $E_{\text{total\_daily\_pv\_production}}$  and  $E_{\text{total\_daily\_load\_consumption}}$  are PV total daily energy production and load total daily energy consumption respectively. Consequently,  $p_{\text{daily}}$  and  $p_{\text{energy\_daily}}$  are subjected to change from one day to another

while  $p$  is a constant for a feeder.  $p_{energy\_daily}$  is dependent on the total energy produced by PV and consumed by load during the day while  $p_{daily}$  depends only on the maximum power produced by PV and consumed by load on that day. In this work, the first definition of  $p$  in (1) is used. No matter what definition is used, the conclusions of this research apply qualitatively.

To simulate future growth of PV, additional PV systems were created by duplicating the specifications (size, tilt, azimuth) of the existing systems with less than 500 kW and moving them randomly to loads that did not previously have a PV system connected. In this way, about 40% of the loads were assigned a PV system. The size of these additional PV systems were scaled by a constant factor to achieve the desired penetration level. Fig. 1f shows the existing plus the newly added PV systems on Feeder A. The target penetration levels are 0, 25, 50, 100, 150, and 200%.

Large and medium-sized PV generators are generally connected three-phase, while the typical connection for the small-sized PV generators is single phase. However, in our simulations all PV systems were connected three-phase; in other words in our simulations 3-phase balanced version of the feeders are used. This is justified in a high PV penetration scenario, as the utility would likely structure interconnection requirements such that an approximate balance between the phases is achieved. Furthermore, the small-sized, mostly rooftop-mounted PV sites connect directly to a bus that has a residential load connected.

### C. Solar Irradiance Data

A network of irradiance sensors or pyranometers at UCSD collects 1 sec irradiance data. These data are normalized by expected clear sky irradiance to yield clear sky indices,  $k_t$ , that are proportional to cloud optical depth [7]. These data were used to assign optical thicknesses to the cloud classes detected by the USI.

Most of the days in the southern California weather can be classified into either clear (large generation, low variability), partly cloudy (medium generation, large variability) and overcast or rainy days (low generation, medium variability). Overcast days are rare, but will effectively reduce PV generation as solar irradiance is typically only at 20 to 50% of its clear sky value. Therefore PV impacts will be lessened. Clear days will result in the largest PV energy generation which impacts line losses, while the impact on tap operations is expected to be small since it takes several hours for PV generation to ramp up and down. Partly cloudy conditions, on the other hand, can strongly impact tap operations as brief periods of large and small generation can alternate up to 100 times during a day. While the ultimate conclusions in this report are based on analyzing a real 90 day timeseries which contains a mix of all conditions, to illustrate the PV impacts in this report we used a partly cloudy day at feeder D on 18-Dec-2015

### D. Net Load Shape Profile and Calculation of True Load

The net power consumption recorded at the substations of all five feeders at 10 min time steps were provided by the host utility and this real net load data that is concurrent with the sky imager observations was used in the simulations. Net load was corrected to determine true load as described in the next paragraph. The average daily load data for each feeder is shown in Figure 3. The profile represents the typical duck-shape profile of California wintertime residential power consumption resulting from large power consumption by residential heating, cooking, and lighting in the early evening. The effect of load disaggregation was investigated in [8].

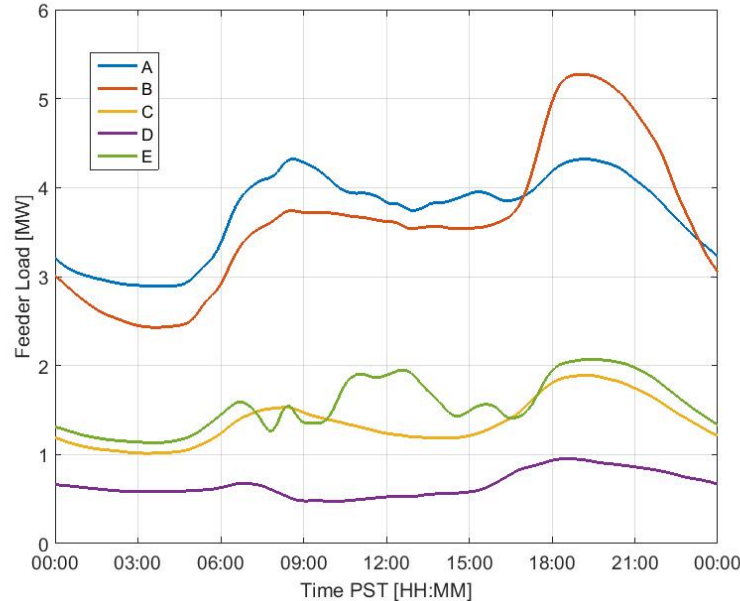


Figure 3 Daily cycle of substation load. Average daily load profile for all five feeders over the 90 day period from substation data provided by the host utility. Substation net load was corrected for existing PV generation (see Fig. 4) to arrive at the data shown in this figure.

On several feeders the net load measured at the substation exhibited strong signs of ‘contamination’ by PV generation such as a reduction in midday net load or even negative net load (Figure 4). For our penetration levels to accurately represent the PV impacts, it was necessary to remove generation from existing PV systems on the feeder from the net load to obtain the true load at 0% PV penetration. The generation from existing PV systems was estimated as follows. The PV fleet capacity and system specifications were obtained from relevant zip codes at the California Solar Statistics website<sup>1</sup>. PV output was simulated using the solar resource determined from the sky imager applied to a PV performance model. Errors in PV generation estimates are introduced in this modeling process since the date of interconnection was unknown. Therefore, the PV fleet capacity was scaled manually to yield reasonable true load profiles and this scaling factor is shown in Table I. Note that since the exact location of the PV systems was unknown, and the sky imager solar resource estimate may be time-shifted due to the process described in Section IIIB, the true load occasionally experienced sharp fluctuations. Therefore a 1 hour moving average was applied to smooth unrealistic short-term fluctuations.

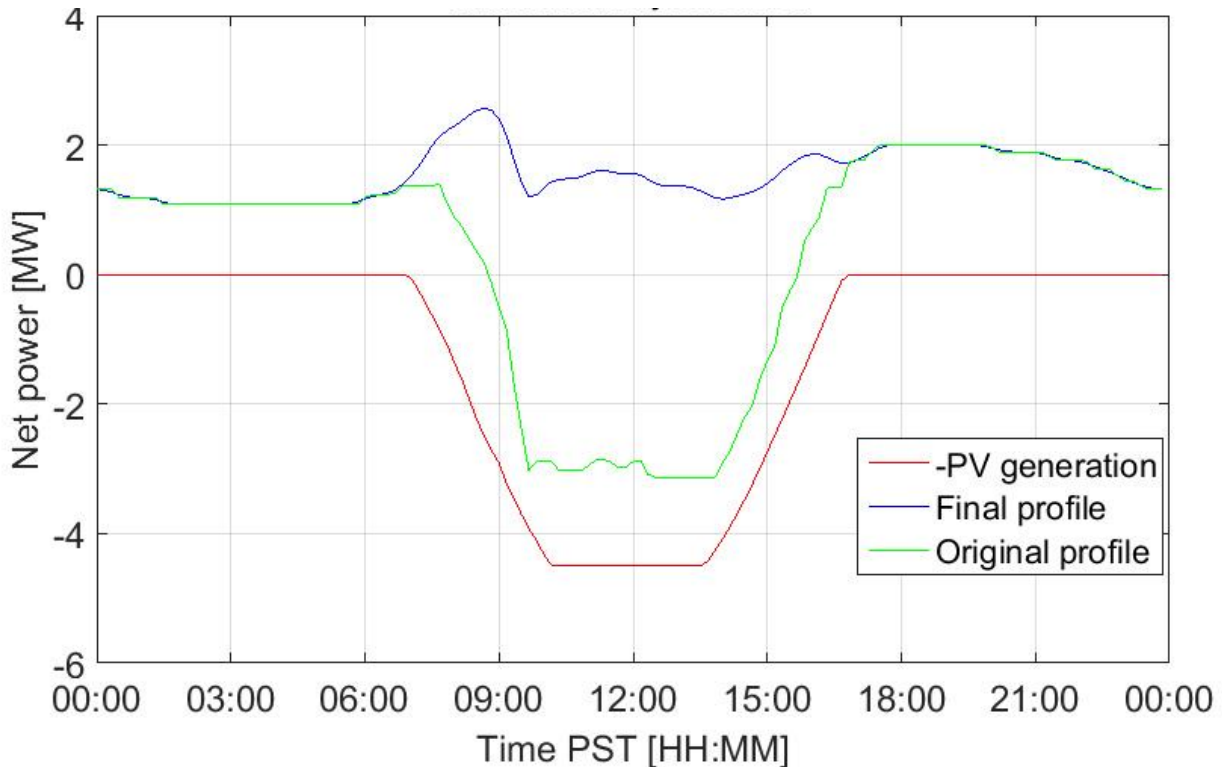


Figure 4 Correction of net load to derive true load. The substation measured (net) load on Dec 6 is shown in green. PV generation simulated based on sky imager solar resource estimates applied to interconnection system data (shown as negative in red) is added to the net load to arrive at the true load (final profile). The true load is used to represent 0% penetration.

### III. REALISTIC, HIGH RESOLUTION AND DISTRIBUTED PV GENERATION PROFILES USING SOLAR RESOURCE ASSESSMENT WITH SKY IMAGER

#### A. Sky imager dataset

The UCSD sky imager (USI) is a high resolution fisheye-lens sky camera that captures an image of the sky every 30 seconds. Three USI's were deployed at feeders A, B, and E. In this report, the sky imager is used in resource assessment or ‘nowcast’ mode, not in forecasting mode. In resource assessment mode, cloud velocity and direction determinations for forecasting cloud locations are not needed. More details are provided in the final report for Subtask 4.3 of this contract.

Since local measurements at feeders C and D were not available, the sky images and pyranometer measurements from La Jolla, CA were spatially translated to the feeder locations. While strong spatial gradients in climate exist in coastal California, winter conditions are usually determined by synoptic weather patterns and are spatially homogeneous. Utilizing the same irradiance data

<sup>1</sup> [https://www.californiasolarstatistics.ca.gov/data\\_downloads/](https://www.californiasolarstatistics.ca.gov/data_downloads/) accessed September 5, 2015.



on some feeders provides insights into the relative importance of feeder characteristics on PV penetration impacts.

Nowcasts were analyzed for periods spanning at least 90 days. The time period of Dec 2014- March 2015 was chosen because all three USIs were operating concurrently and contained the minimum required 90 days of images to analyze. The winter season in coastal California brings about different distinct weather regimes. Frontal passages that bring rain and/or overcast conditions intermittently affect the region. On the opposite end of the cloud spectrum, Santa Ana winds cause dry and clear conditions. Other days may contain partial cloud cover in pre- or post-frontal passages or due to advection of marine air inland. The latter conditions are more frequent at the coastal feeder B than further inland.

### B. Cloud Map and Shadows

Videos showing sky conditions of a sample day can be found at [14]. Each sky image is processed to determine the location of clouds within the image, which are then mapped to a sky grid. The sky image covers a circular sky area with a radius ranging from less than a kilometer to tens of kilometers, depending on the height of the clouds. Due to the fish-eye nature of the camera lens, the spatial resolution of a given area on the shadow maps depends on its distance to the center of the sky image. The resolution is approximately 10 meters near the center and approximately 100 meters near the edge of the sky image. More analysis on this can be found in [8].

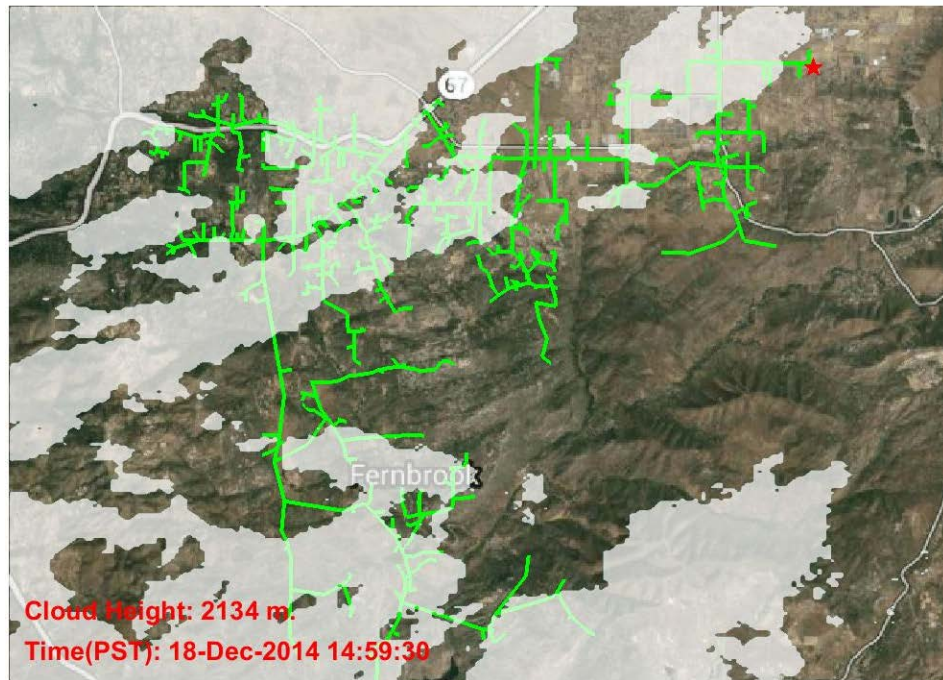


Fig. 5. A snapshot of high resolution cloud shadows over Feeder C showing more than half of the feeder area is covered by clouds, while the remaining area is clear. An animation for Dec 18 can be found at [14].

Processing a raw image from a USI (Figure 5a) to detect clouds in the sky (Figure 5b) is the first step to creating a cloud map. However, the cloud detection method from Ghonima et al. (2012) has issues near the solar region. Notice in Figure 5b near the sun (see Figure 5a for sun position) the cloud detection algorithm works poorly. This is a result of high clear sky red blue ratio ( $RBR_{clear}$ ) values near the solar disk reducing the RBR enhancement caused by clouds. As this research focuses on modeling PV variability of the electric grid impacted by clouds, cloud map production will be modified through horizontal translation and stretching. While the resulting cloud field does not match the actually observed shadows, it preserves the statistics of spatio-temporal variability and mitigates the impact of the solar region.

To project the raw sky image into a Cartesian sky coordinate system, cloud base height (CBH) measurements were obtained from METAR weather reports. METARs are typically generated once per hour (sometimes more frequently) from automated weather observation stations at airports that were 2 to 11 miles away, depending on the feeder.

A geometric transform similar to the pseudo-Cartesian transform of Allmen and Kegelmeyer (1996) was then performed to map cloud information to a latitude-longitude grid at the selected CBH. The resulting “cloud map” is a two

dimensional planar mapping of cloud position at the obtained CBH above the forecast site, centered at the location of the USI (Figure 5c) with a positive linear relationship between CBH and the geospatial coverage of the cloud map.

The main advance in this research is the input of granular solar resource data from sky imager cloud maps. These cloud maps preserve the geographic smoothing effects of real cloud patterns which leads to reductions in aggregate power and voltage fluctuations. However, attempting to reproduce the exact locations of clouds can lead to errors in the solar input as errors in the cloud detection method in sky images are common near the sun and the horizon. While the natural cloud variability of the sky and their impact on PV solar production is preserved statistically, the cloud map is translated with respect to the deployment (Figure 5d) to (1) increase the number of PV systems covered by the cloud map and (2) mitigate the impact of the solar region on the generation of PV profiles. To satisfy both objectives, the following modifications are made to a given image:

- a) To avoid the solar region, the center of the cloud map is moved so the center of the deployment is at 30% of the distance from the sun to the far horizon in the cloud map. Moving the center of the cloud map relative to the sun and far horizon creates a small but insignificant horizontal advection of the cloud maps when compared to cloud speeds. The exception to the previous statement occurs once per day when the far horizon of the cloud map changes from North-West to North-East due to the movement of the sun across the sky, causing a large shift of the cloud map's center in relation to the previous time step.
- b) To increase the number of PV systems covered by the forecast, at low CBH (less than about 500 m, depending on the site) the cloud map is scaled to increase the geo-spatial coverage of the cloud map over the deployment. The diagonal distance of the deployment is used (the diagonal of the rectangle that tightly fits the entire deployment within its geographical bounds) to scale the cloud map to have a minimum diagonal distance of at least 4 times the diagonal distance of the deployment. The scalar of 4 was chosen to prevent excessive scaling, but also to scale the cloud map enough to avoid the cloud map mask at the edges from impacting forecasts. Scaling the cloud map can be interpreted as setting a minimum CBH based upon the size of the deployment.
- c) The clouds are projected vertically to the ground instead of at the slant path dictated by the solar zenith angle. This effectively creates another translation of the cloud shadow field, but it prevents the cloud shadow field from being projected away from the deployment, especially at large solar zenith angles (early morning or late evening) and/or large CBH.

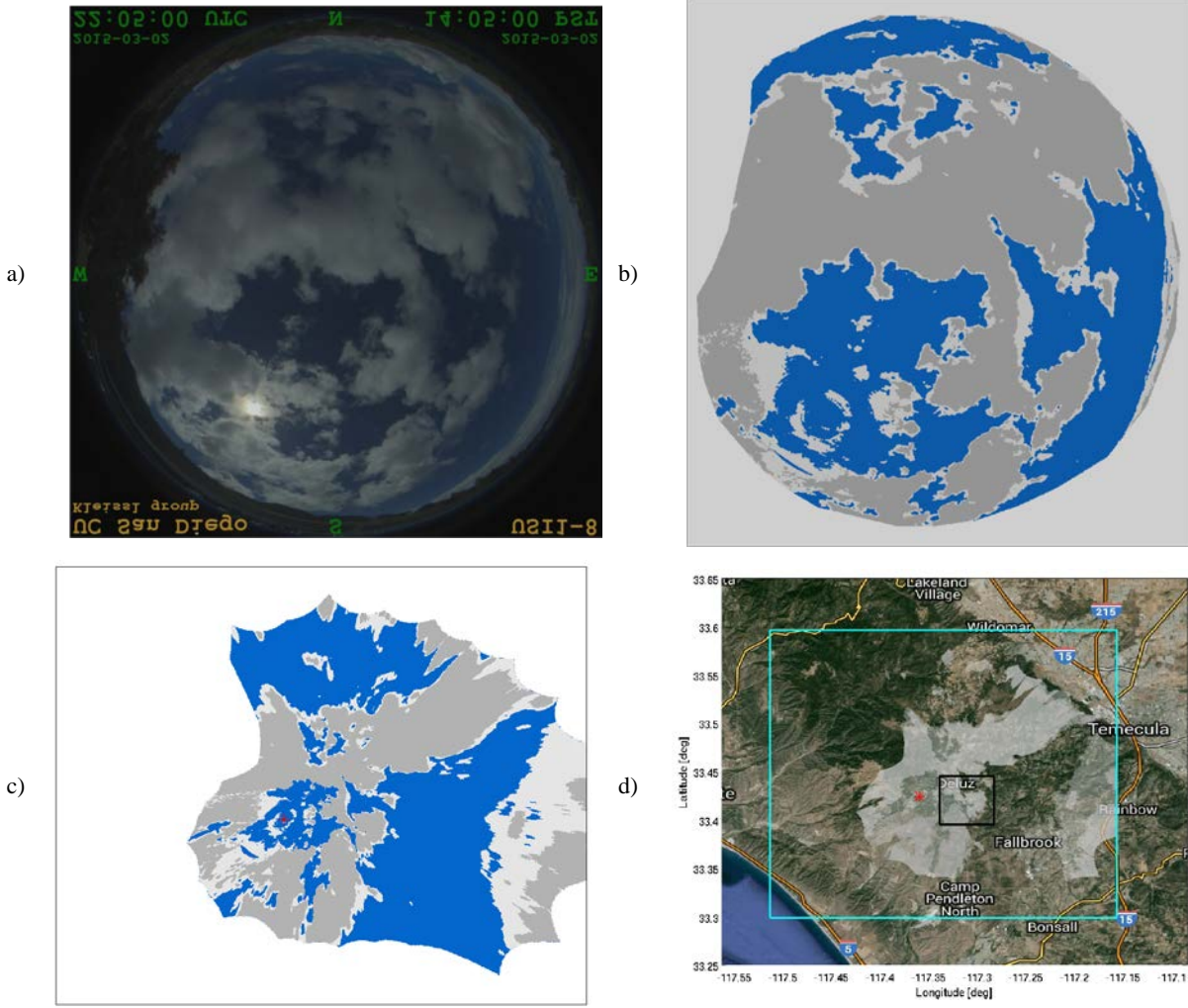


Figure 6 (a) An image of the sky captured by a USI. (b) The cloud decision by the forecast based upon the image in subplot a. (c) The transformation of the cloud decision (subplot b) from spherical to pseudo-Cartesian coordinates to create the cloud map. The red asterisk is the location of the sun. Notice the image is flipped upside down from subplot b. (d) Placement of the clouds (grays) from the cloud map (subplot c) onto Google Maps©. The cyan lines represent the bounds of the cloud map seen in subplot c. The red asterisk is the location of the sun and the black lines bound the ground location where the PV systems are located.

Combining the resulting shadow maps with the known locations of the PV systems on the feeder allows us to determine every 30 seconds whether or not a given PV generator is shaded by a cloud. Unshaded areas on the shadow map receive a high level of irradiance and cloudy areas receive a lower level of irradiance that depends on the optical depth of the cloud. Note that shaded areas can receive considerably more than zero irradiance due to considerable daylight from diffuse horizontal irradiance even on cloudy days. Fig. 4 shows only clear or cloudy levels for visualization purpose while we actually consider three levels of cloudiness: clear sky, thin cloud, and thick cloud. Detail on these levels are explained in the next section. Details on how the opacity of the clouds was estimated can be found in [7]. Because significant spatial differences in irradiance exist, it is crucial to determine unique solar irradiance at each PV site to realistically analyze the impact of high penetration PV on distribution systems.

### C. PV Profile Generation

We calculated global horizontal irradiance ( $GHI(x, y, t)$ ) profiles for each pixel from the series of cloud maps captured by the sky camera and the pyranometer irradiance data. Specifically, we calculated the GHI at each time step as follows:

- Determine the cloud condition (clear/thin/thick) for all the pixels on the ground using the cloud map information. While Fig. 4 shows only clear or cloudy levels for visualization purpose we actually consider three levels of cloudiness: clear sky, thin clouds, and thick clouds [11]. This categorization is used to convert the shadow map to irradiance levels by calculating the clear sky index,  $k_t$ , defined as the amount of irradiation that reaches the ground for each cloud condition.
- Calculate the clear sky index,  $k_t$ , from histograms of the preceding 2-hours of GHI measurements.  $k_t$  is assigned based on the peaks in the  $k_t$  histogram within three ranges: clear sky (0.9-1.1), thin cloud (0.6-0.9), and thick cloud (0.1-0.5) [11]. Using measurements immediately preceding the current time step ensures that the calculated irradiance is based on the most relevant



sky indices. If some cloud conditions are not present during the previous two hours (e.g., if the sky has been clear during the last two hours), then default clear sky indices are used as: 1.06 for clear sky, 0.7 for thin cloud and 0.42 for thick cloud.

- Calculate the weighted clear sky index ( $k_{pv}$ ) for a PV system as the spatial average of the  $k_t$  values of all pixels in the footprint of that PV system as  $k_{pv} = \frac{1}{n} \sum_{i=1}^n k_t^i$ , where  $n$  is the total number of pixels constituting the footprint of the PV system.
- Calculate GHI for each PV system as  $GHI_{pv}^t = k_{pv}^t GHI_{clear}^t$  where  $GHI_{clear}^t$  is the clear sky GHI at time  $t$ .
- Calculate the power output by  $P_{pv} = \frac{GHI_{pv}}{1000 \text{ W m}^{-2}} P_{pv\_rated}$ , where  $1000 \text{ W m}^{-2}$  is the GHI value at which the PV panels are rated and  $P_{pv\_rated}$  is the rated AC power output of the PV system. While this PV power model is simplistic, it is sufficiently accurate to illustrate the effect of representing accurately the spatial PV variability.

Fig. 6 shows a 3-hour GHI profile. For this day, a low and thick cloud layer with large coverage and typical speed was observed. A video of the sky condition on this day can be found at [14]. The conditions were intermittently overcast, clear, and partly cloudy causing large ramps. The GHI profile varies between clear sky conditions (seen as the maximum irradiance levels between 1300-1400 PST), thick cloud cover (from 1220 to 1250 PST) and isolated thick clouds (sharp dips in the irradiance levels between 1400-1500 PST). Fig. 6 shows the existence of location-dependent differences in irradiance levels between the three GHI profiles especially during the partly cloudy period. On the other hand, the overcast and clear condition result in very similar GHI profiles. The three GHI profiles are quite different due to their different locations demonstrating that the geographic diversity effect leads to smoothing of aggregate power ramps.

The model based on sky imager cloud maps yields realistic GHI time series. Comparing to GHI measured by a ground sensor, the sky imager GHI is slightly more variable for the following reasons: (1) Our resource assessment method uses three discrete levels of irradiance output (clear/thin/thick), whereas the range of actual irradiance output measured by the sensors is continuous and  $kt$  can exceed 1.1 during short-lived cloud enhancement events that are of little relevance to PV integration issues. (2) Errors in the sky imager cloud detection algorithms cause, for instance, a thin cloud to be classified as clear sky and that error would cause the forecast to miss a ramp in the GHI profile. (3) The irradiance sensor covers a ground area of only about  $10^{-4} \text{ m}^2$ , while the finest resolution achieved by our sky imager method is  $10 \text{ m} \times 10 \text{ m}$ . Thus, our method averages the generation output, albeit on a scale commensurate with the typical footprint for distributed PV systems. (4) Our solar resource assessment method does not consider the cloud enhancement effect that occurs at cloud edges; cloud enhancement produces irradiance levels that may be greater than the clear sky irradiance level.

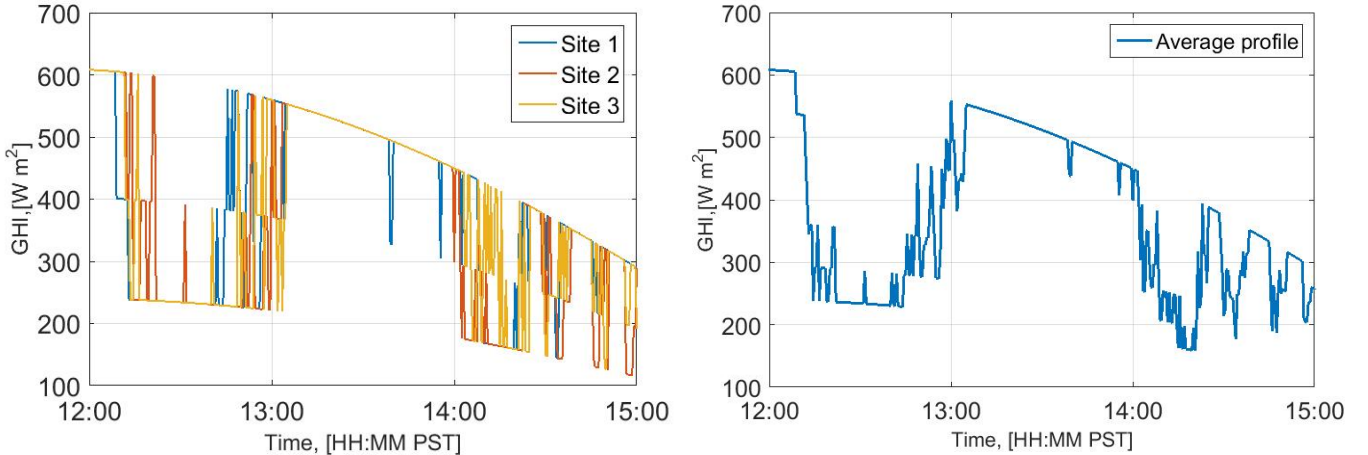


Fig. 7. (a) GHI profiles from 3 different sites of feeder E (see Fig. 1 for locations) from 1200-1500 PST on Dec 18th, 2014. (b) Average GHI from the 3 sites. Some of the GHI variability is mitigated by the differences between the 3 sites.

We calculated the power output of each PV system on the feeder from the GHI profile at the respective PV site and the rated power output of the respective PV system. For example, the GHI profiles for the three systems shown in Fig. 6 were used to generate the power output profiles shown in Fig. 7 for three PV systems with a rated power output of 3 kW, 6 kW, and 33 kW.

Finally, realistic PV generation profiles must account for actual irradiance conditions at the PV locations, which, during partly cloudy days, can be very different at different locations. Moving clouds affect the generated power on two scales: (1) clouds shade part of an array causing shaded and unshaded areas on the same array, and (2) clouds shade part of the feeder causing shaded and unshaded PV sites on the same feeder. The following two sections describe how these two shading conditions are considered.

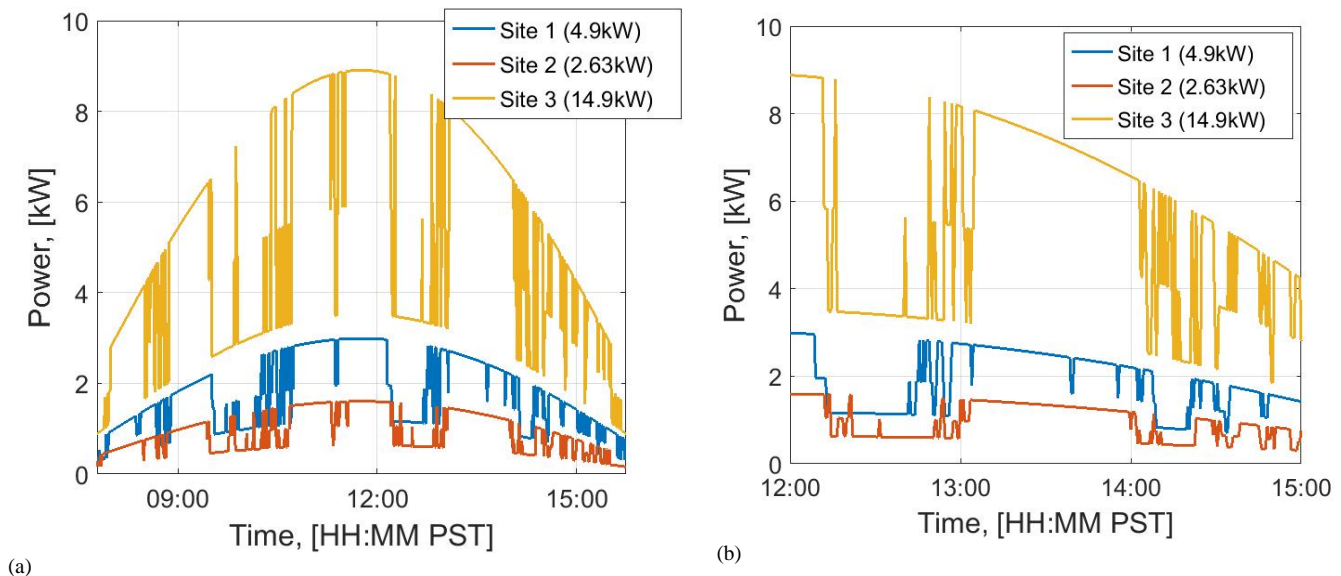


Fig. 8. Power profiles at 3 different sites. (a) Full day comparison. (b) Zoomed in comparison at 1200-1500 PST.

#### D. Clouds Shading Part of a PV Array

The ground area occupied by the PV system depends on the power rating of the generator; that is, PV systems with a higher rating are generally made up of more PV panels that cover a larger area as compared to those systems with a smaller rating. At a given time, some area of a PV array may be shaded by clouds while another part of the same array may be unshaded, a scenario that is more likely to occur on large PV systems due to their larger footprint. The output of a large PV system will not be interrupted immediately when a small cloud begins to pass over and gradually shade the array. Instead, there will be an averaging effect and the cloud-caused variation of the PV power output will be smooth rather than sharp or step-like. On the other hand, the time frame between maximum generation (clear sky) and low generation (array completely shaded by clouds) tends to be much shorter for arrays with a smaller area as it takes less time for a cloud shadow to cover the entire footprint. The finest resolution of the cloud maps is 10 m by 10 m for each pixel in the map. The site with the two 1 MW PV systems located at close proximity on feeder A has a combined footprint of 9 pixels by 18 pixels and is the largest on the feeders. Partial shading was considered using the following methodology:

- estimating the size of the PV area based on its rating,
- establishing the footprint of the PV system based on its size and location,
- determining the shaded and unshaded areas of the PV footprint based on the cloud map,
- calculating the power output for the shaded and unshaded areas of the PV footprint based on the GHI profile for this location, and
- calculating the total power output for each PV system by summing up the power outputs from the PV system's shaded and unshaded areas.

The power generated at a PV site with a large footprint will be smoothed somewhat, but the area of the PV site is small compared to the area of the whole feeder. Consequently the smoothing effect will be more significant when considering the effect of clouds on the total PV generation [10] described in the next section.

#### E. Clouds Shading Part of a Feeder

Some PV sites on the feeder may be shaded by clouds, while others simultaneously experience clear skies. The shaded and unshaded regions are in a continuous flux due to cloud movement. Similar to the case of cloud shading over a portion of a PV array, the net effect of this flux is a smoothing of the feeder PV power output due to the spatial diversity of the PV sites. Fig. 7b shows the dependency of PV generation on location by showing the power output for the same three-hour time frame for three sites at different locations and with different output ratings. It is apparent from the figure that cloud transients (i.e., sharp changes of irradiance levels that cause spikes or dips in the PV power output) occur at different times, for example at about 1415 PST the PV power output of generators 1 and 2 is overcast while generator 3 oscillates between clear and thin clouds. Feeder-wide shading is captured by

- overlaying the cloud map over the feeder area at a given time  $t_1$ ,
- determining shaded and unshaded PV sites based on the cloud map at time  $t_1$ ,
- assigning different power outputs for unshaded and shaded PV systems based on the GHI profile for each PV site, which is determined using the algorithms presented in Sections III.B and III.C,
- solving the OpenDSS circuit for time step  $t_1$ ,

- proceeding to time  $t_2 = t_1 + \Delta t$ , where  $t_1$  is the simulation time step, and
- repeating the process, noting that the cloud map at time  $t_1$  will be different due to cloud movement, until the simulation end time is reached.

#### IV. SIMULATION SCENARIOS AND SETUP

The resource assessment technique outlined in Section III was used to produce solar power data for distribution power simulations for the five distribution models introduced in Section II.A. Different scenarios were examined:

1. **5 Feeders:** Simulations with all five feeder models (described in Section II.A) to study the dependence of PV impacts on feeder topology. Multiple individual and realistic PV profiles are used for all five feeders.
2. **PV penetration levels** at 0%, 25%, 50%, 75%, 100%, 150%, 200%.
3. **90 days:** For each of the above setups, 90 day simulations with 30 second simulation time step were run. Results are illustrated through a case study using a partly cloudy day complemented by aggregated results for the full period.
4. **'X-single' and 'X' (multiple) PV profiles configurations:** To investigate the impact of using multiple individual and realistic PV profiles versus a single common profile for all PV systems, two other special configurations were set up for all five feeders: (1) 'X-single' configuration (with X as one of the five feeders, A-E) using a single PV profile to force all PV systems; and (2) 'X-multiple' configuration with multiple PV generation profiles specific to each system created using the method in Sec. III. The difference between the uses of single versus multiple PV profiles is best shown by the net power fluctuation frequency and magnitude recorded at the substation in Fig. 8.

Thus, the total number of simulated scenarios is 5 feeders x 2 scenarios x 7 penetration levels = 70.

#### V. RESULTS AND DISCUSSION

In this section, the analysis is organized as follow: (1) comparison of impacts of high PV penetration on reverse power flow, energy consumption, line loss, tap operations, and voltage levels among the five feeders, which includes two configurations (single and multiple) A; (2) impacts of using aggregated versus disaggregated PV profiles as input to the simulations.

The difference between single and multiple can be captured by examining the net power consumption recorded at the substation (see Fig. 8). The disaggregated PV profiles used in E-multiple creates a more realistic net profile with some smoothing effect from summing up the output power from PV systems in different locations. The E-single net power profile suffers more frequent ramps and larger ramp magnitudes. More detailed analysis on the effect of using aggregated versus disaggregated profiles will be shown in subsection F. The results in the preceding sections are all based on the multiple configuration, unless otherwise noted.

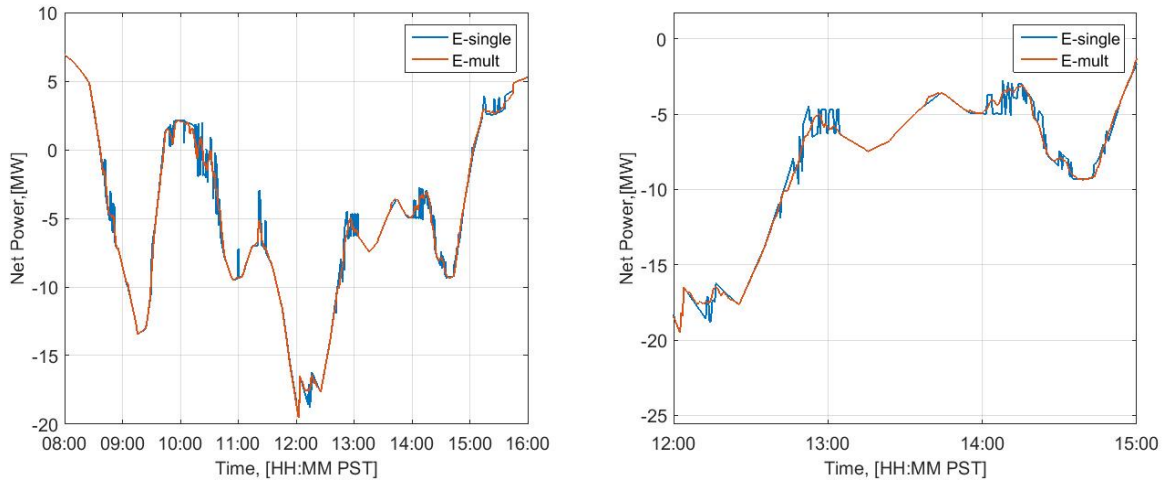


Fig. 9. Net power consumption recorded at the substation for E-single and E-multiple (a) from 0800 to 1600 PST (b) from 1200 to 1500 PST, on Dec 18<sup>th</sup> 2014. For both cases the PV penetration level used was 200%. Negative values represent backflow from the feeder back to the transmission system. The use of multiple PV profiles reduces the frequency and magnitude of net power fluctuations.

### A. Reverse Power Flow

Fig 9 shows the difference in net active power consumption between 0% and 200% PV penetration levels on Feeder C. It can be seen that during daylight hours, PV system power output creates large difference in net power in comparison to the 0% case. Depending on the penetration level, reverse power flow can occur. In the 200% case, it can be seen that the net power at substation is negative (indicating reverse power flow) most of the time from 08:00 to 15:00 PT.

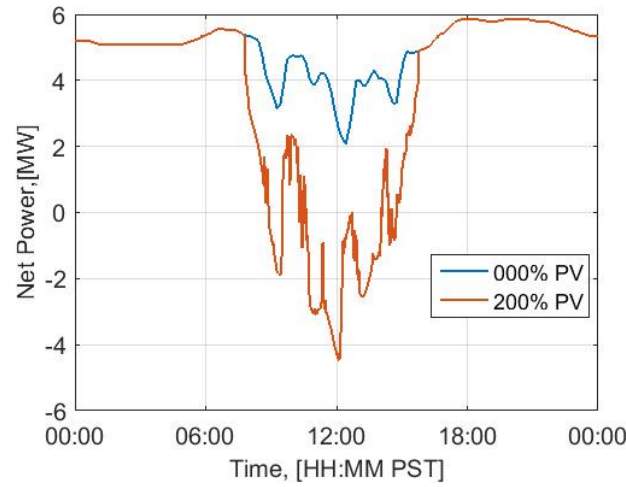


Fig 10. Net active power consumption recorded at the substation of Feeder E with aggregated PV profiles (scenario E-single) on Dec 18<sup>th</sup>, 2015 with PV penetration levels of 0 and 200%. Reverse power flow (negative value) occurs between 9:04 and 14:47 PT at the 200% PV penetration level. The current penetration level is estimated to be 180%.

### B. Energy Consumption Savings

Net energy consumption, the active power delivered by the substation to supply the load demand on the feeder, is significantly reduced as the PV penetration level increases. At 200% PV penetration, the PV power output satisfies about the total net energy needed for 5 feeders. If the outside generation units are fueled by conventional, non-renewable resources (i.e., fossil and radioactive fuels), this reduction leads to significant savings of these resources. It is noteworthy that the energy saving percentage curves for the feeders varies, which is the result of the definition of the PV penetration level based on rated power and rated load rather than energy produced. Feeder A has the least savings of the 5 feeders due to its long feeder length which causes more losses during power flow. It can also be seen that – as expected – the power reduction or savings is linearly proportional to the PV penetration level.

The total energy production between single and multiple were forced to be identical. The PV system that was used to supply the ‘single’ profile may have some deviations from the average of the ‘multiple’ systems and skew the ensuing results for losses, tap changes etc. Therefore the single profile was calibrated to be the same as the average of all ‘multiple’ profiles.

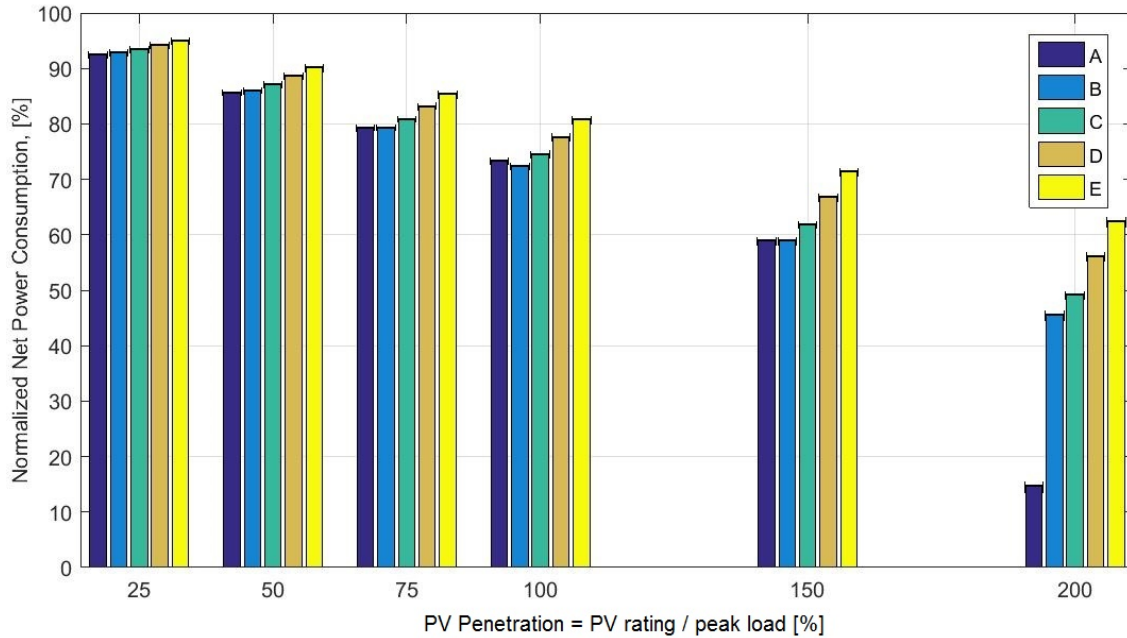


Figure 11-Normalized (0% penetration = 100% net power) net power consumption for the 90 days. The net load was forced to be the same for both configurations single (black marker) and multiple (bar).

### C. Distribution Line Losses

As PV penetration increases from 0%, the line losses first decrease as local energy demand is met by local PV output (Fig. 11). However, as PV penetration passes a certain level, the power generated by PV flows further and further to meet local demand or even flow back to the substation, which causes the line losses to increase again. For the relatively long feeder A, the minimum loss occurs at 50% PV penetration while for the other four feeders, it happens at 100% PV penetration. For most of feeders (except D) the loss at 200% PV penetration is even larger than that at 0% due to large amount of reverse power flow from excess PV power outputs.

Fig. 12 illustrates that the line power loss observed at 200% penetration level is much lower than loss at 0% penetration level during early morning (7:00 -9:00 PT) and late afternoon (14:00 -16:00 PT) when less power output from PV arrays supplies local loads without causing reverse power flow. In the middle of the day, when the amount of solar irradiance is at the peak, PV output in 200% case exceeds the local demand, which causes reverse power flow and increases line losses compared to the low-irradiance hours.



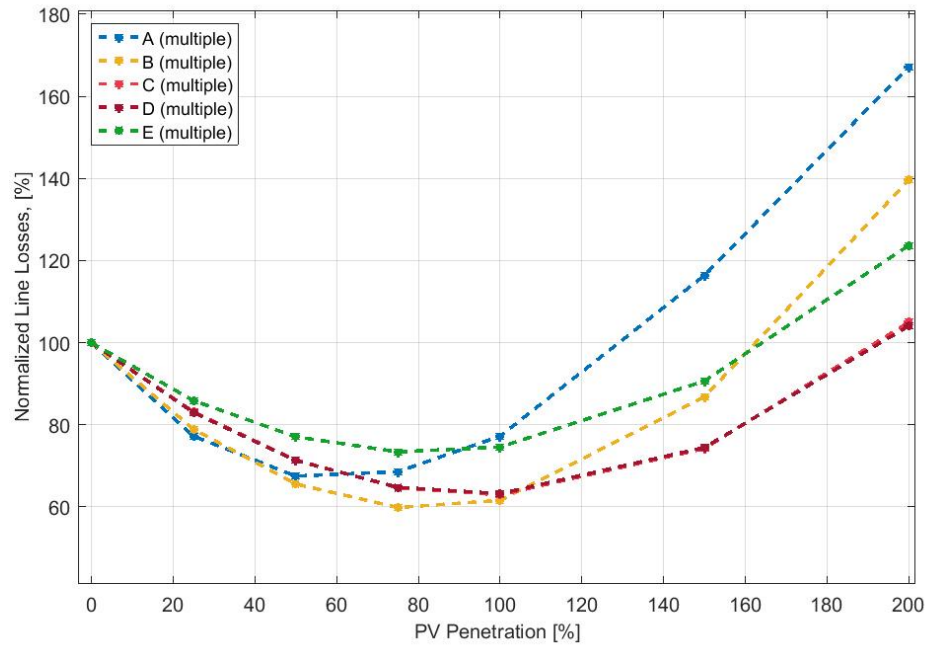


Fig. 12. Normalized line losses with increasing PV penetration relative to the base case of 0% PV penetration for the 90 days of simulation. There is a vertex point (100% for Feeders B, C, D and E and 50% for Feeder A), after which the reduction in line losses decreases as PV penetration increases.

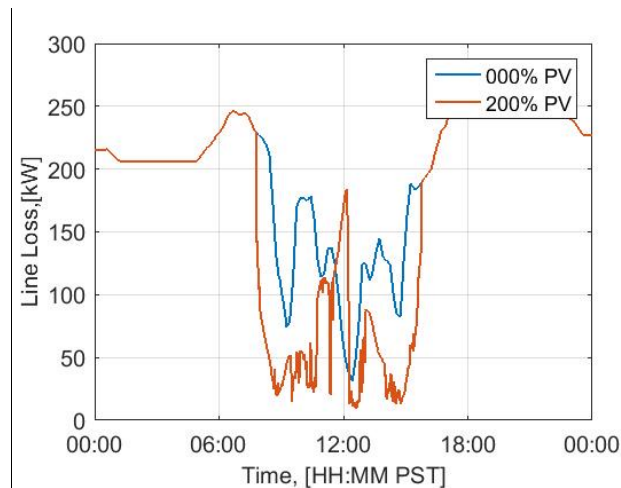


Fig. 13. Total line loss during the day recorded on rural Feeder E with aggregated PV profiles (scenario E-single) on Dec 18th, 2015 with PV penetration levels of 0 and 200%.

#### D. Voltage Fluctuations and Over-voltages

Voltage setpoints for the substation and feeder voltage regulators significantly impact the minimum and maximum voltages on the feeder. Consistent with the settings provided by the utility in the validation files, the following settings were used:

- A: All VRs (including substation) are set at 1.02 for validation purpose but are set at 1.0 for all simulations to improve convergence.
- B: Substation at .98. No secondary VRs.
- C: Substation at 1.01, other voltage regulators at 1.0.
- D: Substation at 1.01. Other VRs at 1.0.
- E: Substation at .99. Other VRs also at .99.

Since the impacts of PV are limited to the daylight hours we restrict the analysis of voltages and tap changes to the period when there is PV generation, generally from shortly after sunrise to shortly before sunset. The variability of the sun-up period is considered in this analysis and just data between sunrise and sunset for each day and site were considered. Lower voltages are expected to occur during the evening load peak. Fig. 13 shows the significant difference in voltage level along the feeder between

two cases: 0% and 200% PV penetration. During daylight hours, power production from PV systems raises the voltage levels of the feeder in general (Fig. 13a). Near noon the voltage is as high as 1.04 p.u. voltage on feeder E for 200% penetration of PV. On the other hand, the minimum voltage increases relatively even further and is brought to a level that is nearly compliant with the 0.95 ANSI standard. The voltage also varies along the feeder according its length, the feeder E has two transformers; one located in the substation and the other located approximated 10 km from the first. The Fig. 13b shows how the voltage drops along the transmission lines, until the second transformer elevates it, which was below the 0.95 ANSI standard.

Generally, voltage ranges for feeders B, D, and E are within the 0.95-1.05 p.u. voltage range even up to 200% PV penetration (Fig. 14 for shows feeder E as an example). However, feeder A's voltage exceeds 1.05 p.u. for PV penetration levels higher than 100%. As expected, maximum voltage levels are generally observed around noon times when the level of solar irradiance is at its highest level.

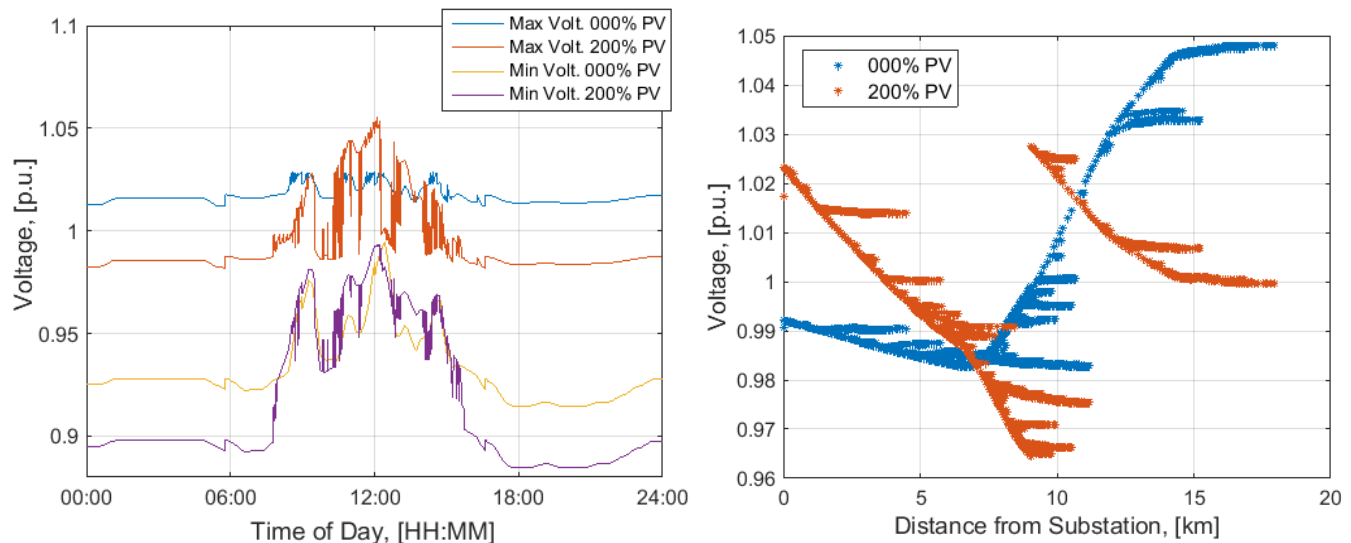
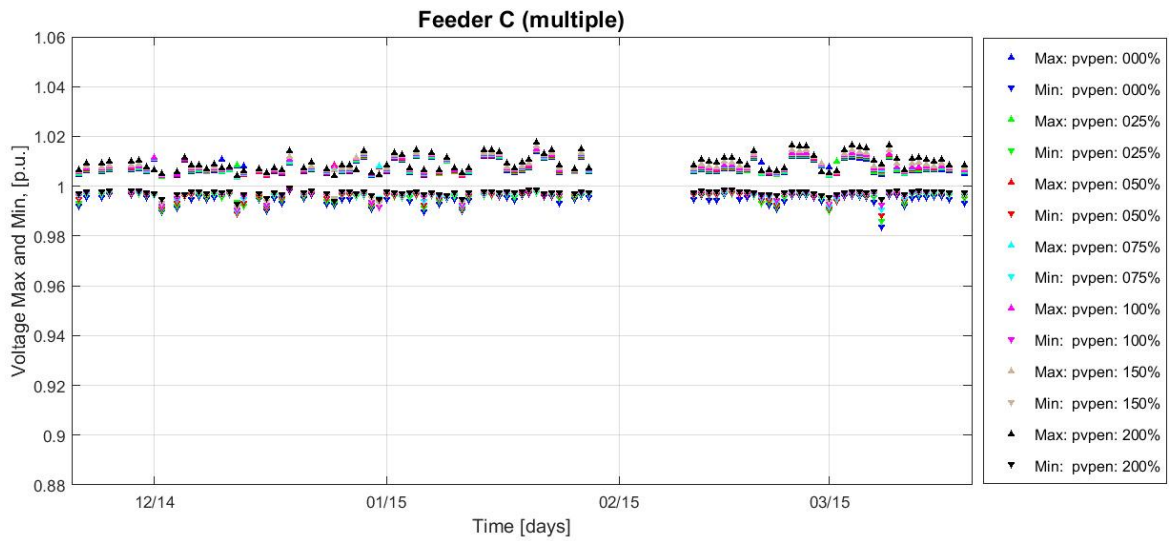
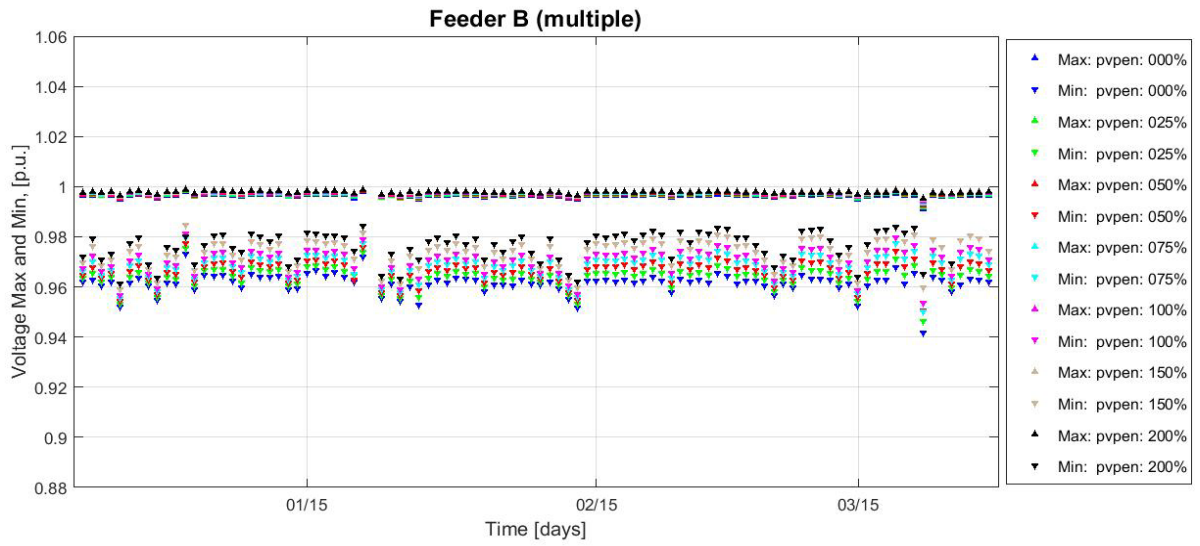
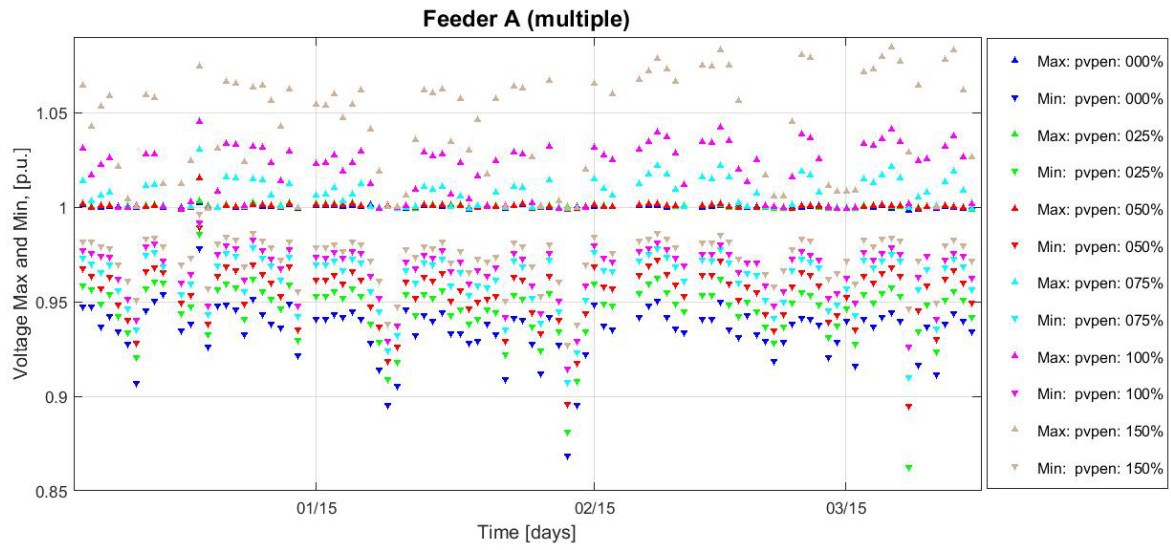


Fig. 14. (a) Voltage fluctuations during the partly cloudy day on Dec 18 for E-multiple at 200% PV penetration. The current estimated penetration level is 180%. The maximum voltage does not exceed the 1.05 ANSI limit. (b) A snapshot of the feeder voltage profile at 11:45:30 PT, when the highest level of GHI were measured at this day. The maximum voltage occurs at the end of the feeder as a result of reverse power flow. The 0% case was run for a substation voltage setpoint of 1.02 which is more realistic for 0% PV penetration.

It can be concluded that for all feeders, as PV penetration increases, the voltage range increases with a rate that depends heavily on the network topology and characteristics. Feeder A experienced the most significant voltage violations even at low levels of penetration due to its long feeder length, high load demand, and two large PV sites at the end of the feeder. No voltage violations were recorded on B, C, and D even at 200% penetration due to their small size, short feeder length, and low customer density. Therefore, these networks have higher hosting capacity for distributed generation and are ideal candidates for hosting high PV penetration. This is an important finding because it suggests that the voltage excursions caused by the presence of PV systems depend highly on feeder's topology and characteristics such as its coverage area, feeder length, urban or rural type, load demand, and distribution of load and distributed generation [17]. Concurrent analysis from another CSI RD&D grantees – albeit without sky imager solar resource data – also reached similar conclusions regarding the important of feeder topology and characteristics. In addition shorthand formula for hosting capacity estimation was developed.<sup>2</sup> Additional work is ongoing under the CSI RD&D4 program by EPRI (Analysis to Inform Grid Integration Rules for PV) and SCE (Advanced Distribution Analytic Services Enabling High Penetration Solar PV).

<sup>2</sup> Smith, J., Alternatives to the 15% Rule Modeling and Hosting Capacity Analysis of 16 Feeders, Technical Update to the California Solar Initiative RD&D program, EPRI, Palo Alto, CA: 2015. 3002005812. Available online at [http://www.calsolarresearch.org/images/stories/documents/Sol3\\_funded\\_proj\\_docs/EPRI/Modeling-Analysis-16-Feeders\\_3002005812.pdf](http://www.calsolarresearch.org/images/stories/documents/Sol3_funded_proj_docs/EPRI/Modeling-Analysis-16-Feeders_3002005812.pdf).



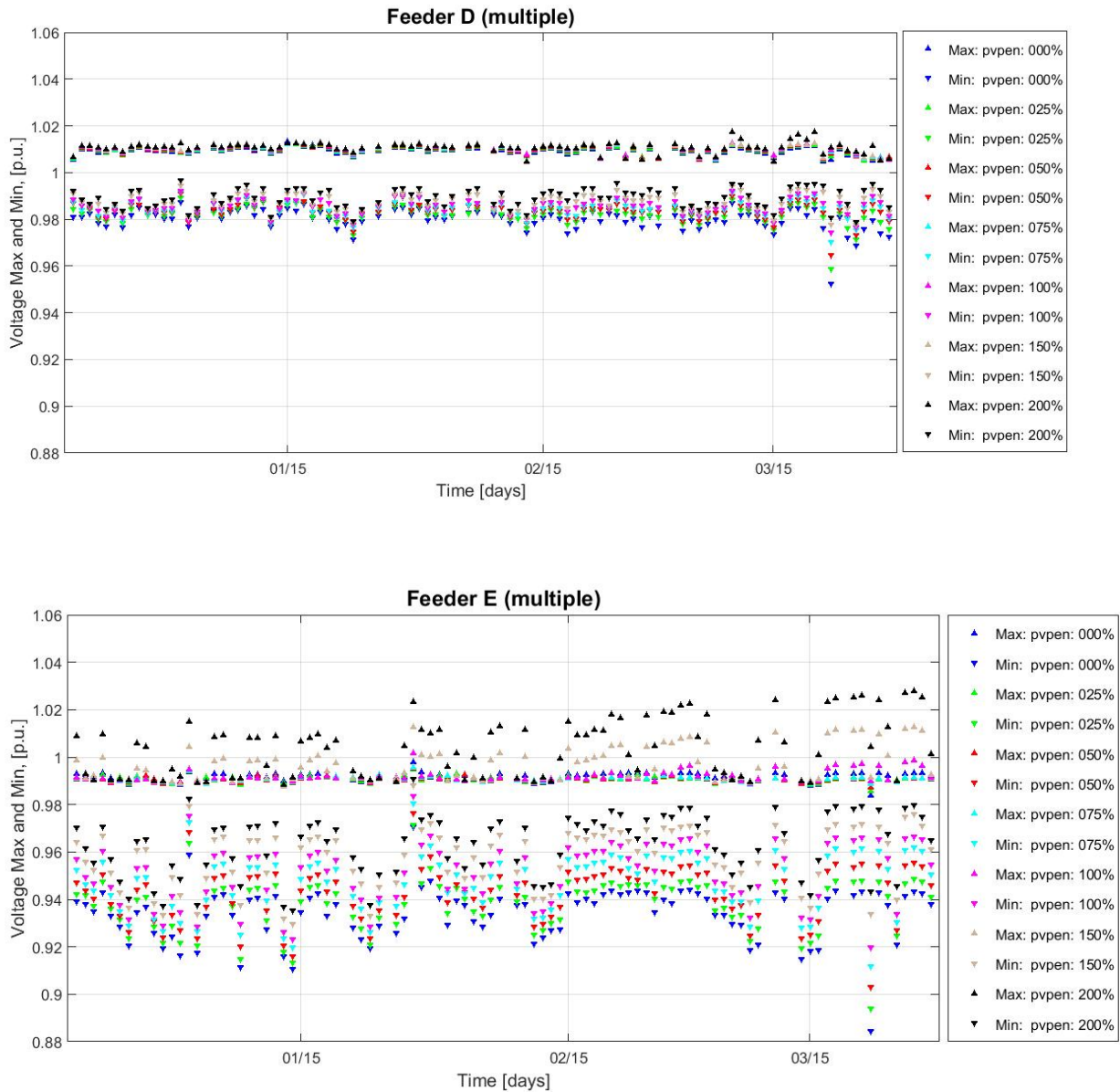


Fig. 15. Maximum and minimum voltages on 90 days for day time for all feeders at different penetration levels. The results for feeder A with 200% PV penetration are not shown in the figure, because simulations did not converge on 75% of the days since line thermal limits were reached,

### E. Tap Operations

In order to reduce the voltage fluctuation in a power grid, transformers and voltage regulators are equipped with On-Load Tap Changers (OLTC) which are programmed to change their tap position to keep voltage levels along the feeder within permissible limits. However, there are some concerns with the operation of OLTC's while performing tap changing processes.

The main parts of an OLTC is the diverter switch which is responsible to effectively manage the tap operation process without disconnecting the current flow of the transformer. Therefore, switching arcs are inevitable on the main switching and transition contacts of the diverter switch. These arcs creates carbonization of the switching oil and cause contact wear. Since diverter switches operate within 40 to 50 ms, the mechanical elements such as springs, braided contact leads etc. are exposed to remarkable stress during every single tap changing event.

Within a tap changing process where the tap position is supposed to change for more than one step, the diverter switch is not able to skip the intermediate steps. Instead, it starts from the initial position and gradually moves through the intermediate steps until it settles on the final position. Thus, the stress on inverter switch is a function of not only the number of distinct tap operations, but also the number of taps changed in one operation which is identified as the number of tap operations, hereafter.

According to the mechanical and electrical stresses which OLTC experiences in each tap operation, the number of tap operations is one of the main parameters to define the schedule of OLTC maintenance. For example, in [18]-[19], preventive maintenance is recommended to be performed on the tap changer after one million tap operations.

Regarding the intermittent power output of PV panels and its essential effect on grid voltage, especially for high penetration of PV, high volume of tap operations are expected. Therefore, it is crucial to investigate the number of tap operations as one of the parameters affecting the distribution system operation cost.

As an example, Fig. 15. shows the voltage observed on substation transformer and transformer #4 on feeder A. Fig. 15. shows that transformer #4 on feeder A decreases the voltage during the daytime when excess PV production occurs and increases the voltage in the evening during the net load peak. In both cases, there is large difference in the operation of the transformers during daylight hours between 0% and 200% PV penetration levels. Due to the fluctuation in PV power output in partly-cloudy weather condition, extra operations were needed to keep voltages of the set points, at desired level. A comparison between Fig. 15a and Fig. 15b demonstrates that the number of tap operations of the secondary transformer is significantly higher than that of the substation transformer. It is mainly because the secondary transformer is closer to the large PV sites and exposed to higher voltage excursion than the substation transformer which sees the net power of the whole feeder. The substation transformer performs the lowest number of tap operations because it is the closest transformer to the transmission network, with a voltage close to one per unit, and experiences the least level of voltage fluctuations. Thus, the number of tap operations needed at the substation transformer is less than at the secondary transformer #4.

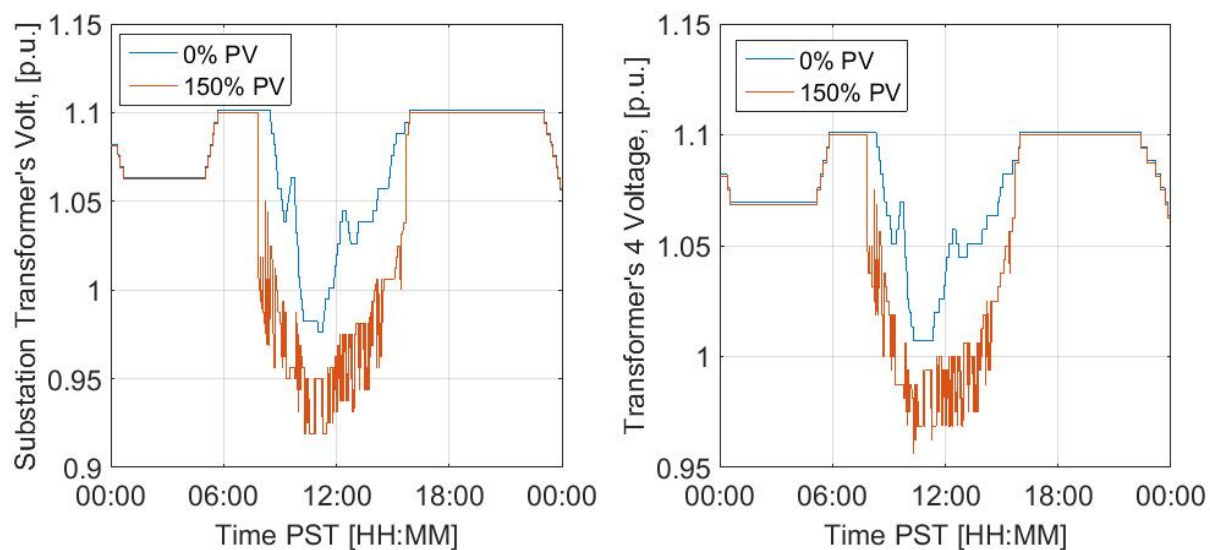


Fig. 16. Voltage during the day recorded on rural Feeder A with aggregated PV profiles (scenario A-single) on Dec 18<sup>th</sup> 2014 with PV penetration levels of 0 and 150%. The impact of the PV systems manifests during daylight hours when there is difference in tap positions between the two cases. A. **Substation** transformer. b). Secondary transformer #4 (Fig. 1)

Fig. 16 shows the average number of tap operations per day for each feeder. Feeder A experienced a very high increase in the number of tap operations in comparison to the other feeders due its larger number of transformers and voltage regulators (Table I) as well as larger voltage variability (Fig. 14). There are barely any tap operations on feeder B even at 200% PV penetration since the feeder stiffness causes small voltage variability. For feeder C, D, and E tap operations increase from 1, 13, and 30 at 0% penetration to 4, 30, and 100 at 200% penetration.



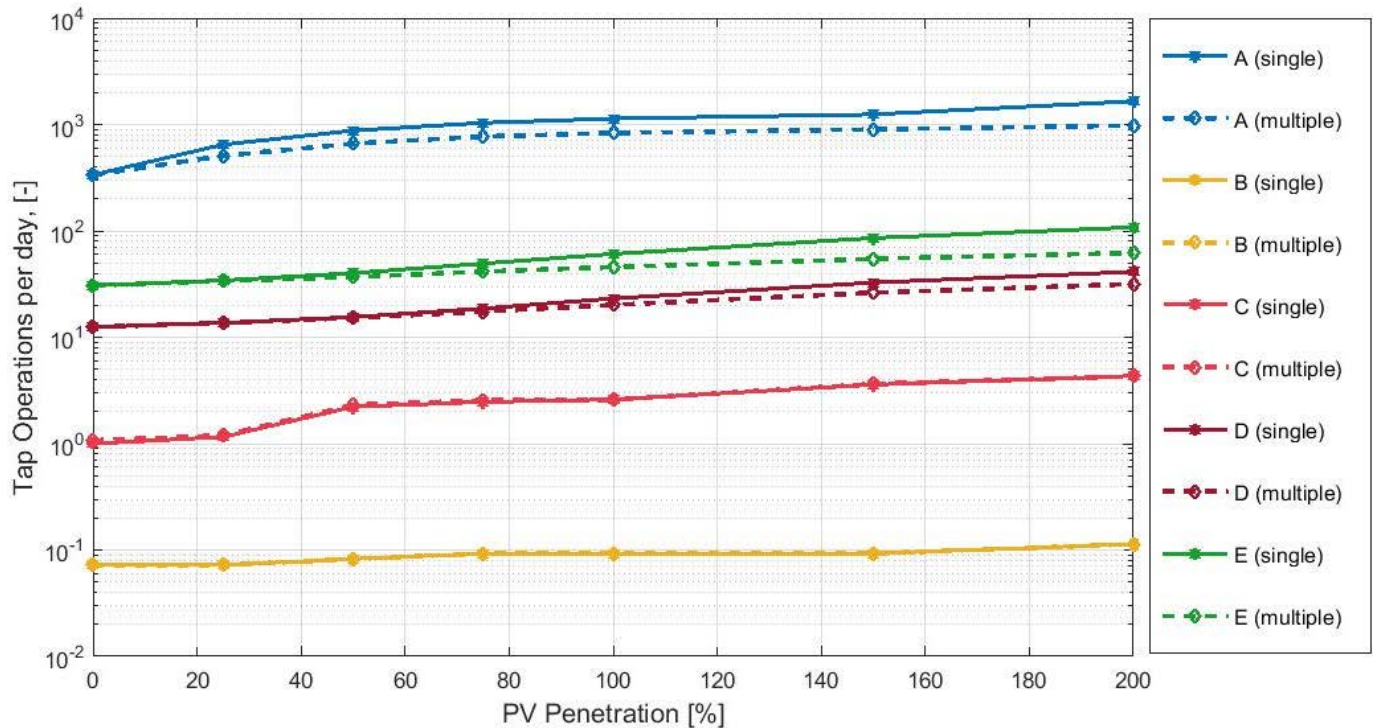


Fig. 17. The average number of tap operations per day during daytime. At 0% penetration feeders A, B, C, D, and E have 336, 0, 1, 13, 30 tap operations, respectively. The number of tap operations for feeder B in the single and multiple scenarios are identical and independent of PV penetration level. An additional tap operation may occur at night, but only daytime tap operations are considered here.

#### F. Aggregation vs. Disaggregation of PV Irradiance Profiles

In impact studies of high penetration PV on distribution feeders it is common to assign the same power output profile to all PV systems on the feeder for reasons of simplicity and lack of data. However, this method of aggregating PV irradiances introduces errors into the simulation because it does not consider the spatial variability in power output caused by cloud shadows across the feeder. The novel approach presented herein disaggregates PV irradiances in high temporal and spatial resolution and thus considers this spatial variability in a highly realistic manner. This approach is much closer to reality and therefore yields more accurate results.

A key difference between the use of aggregated and disaggregated PV profiles is in the net power fluctuation frequency and magnitude (see Fig. 9). On the partly cloudy day (Dec 18th), the total power demanded by the feeder (as measured at the substation) fluctuated significantly more when the aggregated profile was used. This is unrealistic, especially for feeders with large footprints as the correlation between GHI between sites decreases exponentially with distance. Fig. 9b illustrates that the fluctuations in power for disaggregated PV profiles (C-multiple) is significantly less severe in both magnitude and frequency due to the averaging or smoothing effect of having many individual generation profiles. The severe fluctuations in C-single in total power are artifacts caused by the use of the single aggregated profile. Power output from individual PV systems ramps up and down due to local cloud conditions, but the use of an aggregated profile causes PV systems over the entire feeder to ramp coincidentally, which is unrealistic for feeders with a sufficiently large footprint. This difference will have significant impacts for those studies or policies that concern power ramp rates and magnitudes.

A result of the more intermittent PV power output, the single PV profile configuration overestimates the line losses (normalized using the 0% PV case in Fig. 17) in the feeder. The overestimation amount is relatively small even at very high PV penetration levels typically about 1.5% overestimation at 200% penetration.

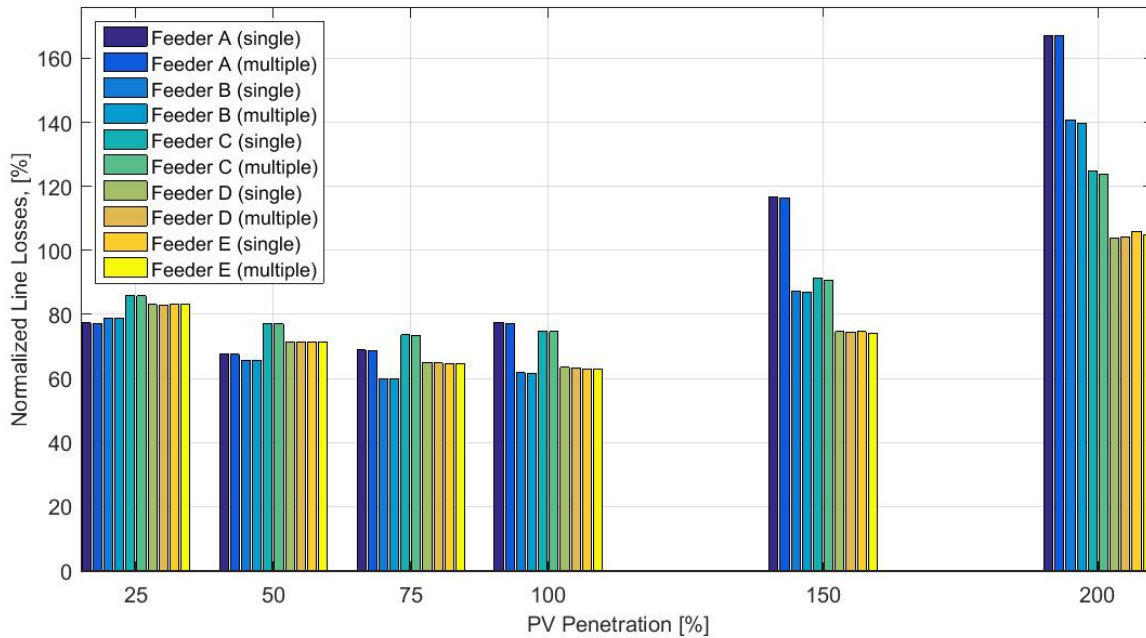


Fig. 18 Normalized line losses relative to the 0% penetration case for all five feeders with single and multiple PV profiles configurations for the 90 day period. For the 100% case the losses for 'multiple' are [0.37, 0.25, 0.41, 0.30, 0.03]% less than for 'single'. For the 200% case the losses for 'multiple' are [0.08, 0.01, 0.98, -0.09 0.86]% less than for 'single'.

Peak voltages generally occur at minimum net load which occurs during midday at high PV penetration. If the midday period is partly cloudy one would expect that the peak PV generation and therefore the maximum feeder voltage are also artificially enhanced if a single PV profile is considered. On the other hand, for clear and overcast days, no difference would be expected. Therefore the multiple scenario is not expected to consistently reduce peak voltages.

However, the primary effect of distributed PV profiles is the reduction of PV power ramp rates and ramp magnitudes that is expected to lead to a reduction in voltage regulator actions which directly affects the lifetime of voltage regulators and transformers. Indeed the number of tap operations on all feeders decreases substantially (Fig. 18) with the exception of feeder B which has very few tap operations (much less than 1 per day) at all PV penetration levels. The ratio of overestimation increase with penetration level from about 8% at 25% penetration to about 46% at 200% penetration, on average for feeders A, C, D, E. The largest overestimation occurs on feeders A and E with about 70% too many tap changes at 200% penetration. Again for clear and overcast days, no difference between 'single' and 'multiple' would be expected; therefore the increase in tap operations on partly cloudy days must be dramatic. This shows the unique feature of our approach in which we model the PV production output more realistically and estimate the actual tap changing operations more accurately, especially during cloudy condition.

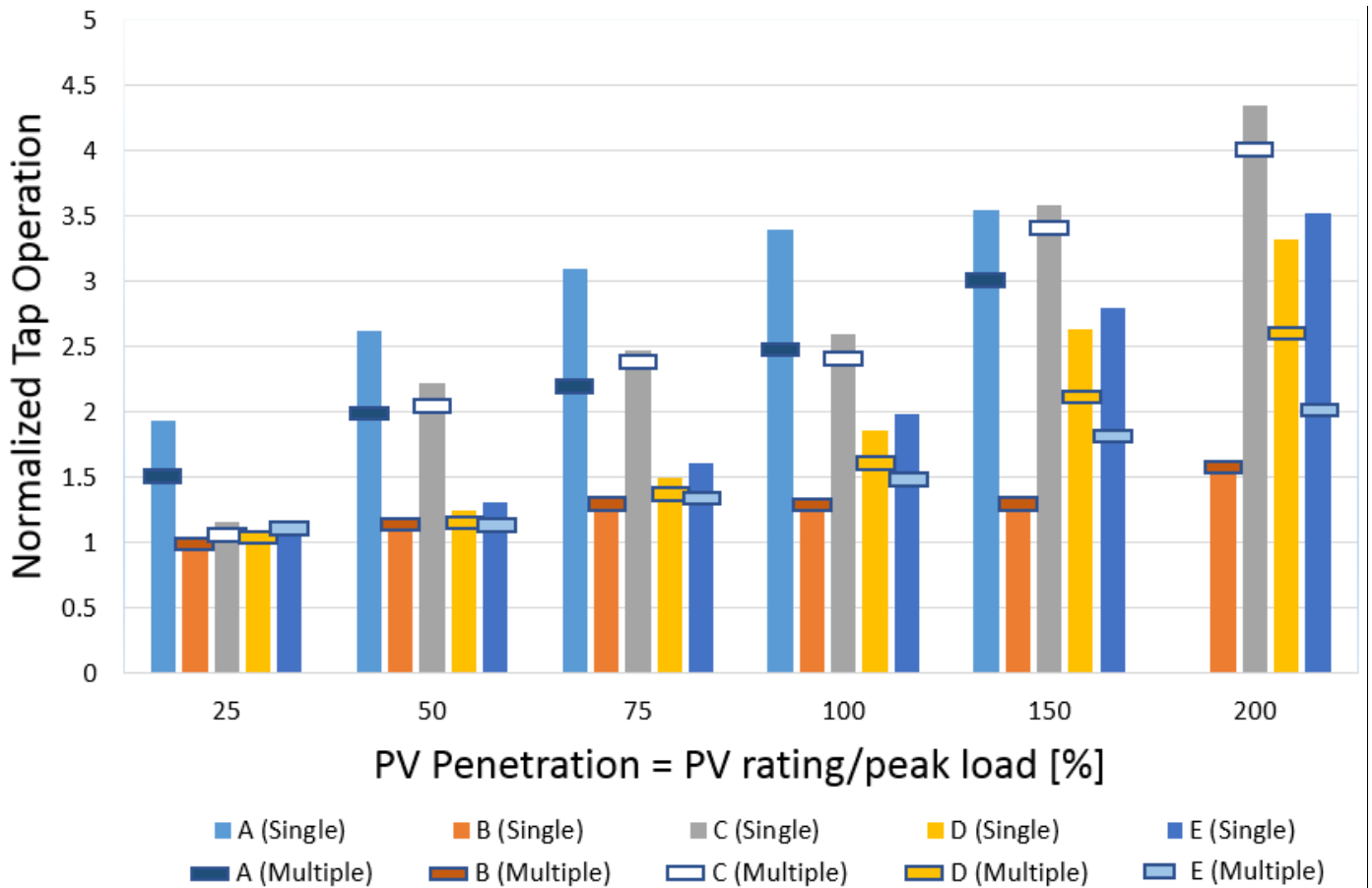


Fig. 19. Normalized tap operations (tap operations at 0% PV penetration = 1) of five feeders with single and multiple PV profiles configurations for the 90 day period. Only tap operations executed during day time were considered in this histogram.

## VI. CONCLUSIONS

In this report, we have proposed a new approach to study the impact of high PV penetration on a distribution network and its hosting capacity. The proposed method combines high resolution resource assessment using sky imagery with power system simulation on real distribution models to study the impacts of up to 200% PV penetration level on voltage excursions, line losses, and tap changing operations. We capture the unique temporal variation in power generated by each PV system in a highly realistic fashion.

The results from simulations show that the topology and allocation of loads and resources on the feeder play an important role in the ability of the feeder to host high PV penetration. Adverse impacts associated with high PV penetration were observed on feeder A with long length and high load demand. Thus it has trouble hosting 100% PV penetration, while feeder E can host up to 200% PV penetration. Feeder B, C and D can potentially host even higher PV penetration levels since their voltage levels are well within the desired range even at 200% PV.

It was shown that disaggregated PV generation profiles should be used in impact study of high PV penetration, especially when factors like tap operations and power ramps are of concern. Using an aggregated PV profile overestimates significantly the number of tap operations and power ramp rates and magnitudes. Disaggregated PV profiles can be achieved deterministically from either real PV measurement data (which is not always available due to large and expensive required infrastructure) or the use of solar resource assessment using sky imagery as proposed.

For the follow-on Task 4.4, we are designing various schemes utilizing solar forecasting in conjunction with control of load tap changers to mitigate the impacts of high penetration of distributed resources and to maximize the benefits of solar energy.

## REFERENCES

- [1] M. ElNozahy and M. Salama. (2013, May). Technical impacts of grid-connected photovoltaic systems on electrical networks – A review. *Journal of Renewable and Sustainable Energy*. [Online]. 5. Available: <http://dx.doi.org/10.1063/1.4808264>

- [2] R. Passey, T. Spooner, I. MacGill, M. Watt, and K. Syngellakis. (2011, October). The potential impacts of grid-connected distributed generation and how to address them: A review of technical and non-technical factors. *Energy Policy*. [Online]. 39 (10), pp. 6280-6290. Available: <http://dx.doi.org/10.1016/j.enpol.2011.07.027>
- [3] M. Thomson and D.G. Infield. (2007, March). Impact of widespread photovoltaics generation on distribution systems. *Renewable Power Generation, IET*. [Online]. 1 (1), pp. 33-44. Available: <http://dx.doi.org/10.1049/iet-rpg:20060009>
- [4] S. Ali, N. Pearsall, and G. Putrus. (2012, March). Impact of high penetration level of grid-connected photovoltaic systems on the UK low voltage distribution network. Presented at International Conference on Renewable Energies and Power Quality. [Online]. Available: <http://www.icrepq.com/icrepq12/368-ali.pdf>
- [5] J.H.R. Enslin (2010, July). Network impacts of high penetration of photovoltaic solar power systems. Presented at the Power and Energy Society General Meeting, 2010 IEEE. [Online] Available: <http://dx.doi.org/10.1109/PES.2010.5589675>
- [6] M. Lave, J. Kleissl, and E. Arias-Castro. High-frequency irradiance fluctuations and geographic smoothing. (2012, August). *Solar Energy*. [Online]. 86 (8), pp. 2190-2199. Available: doi:10.1016/j.solener.2011.06.031
- [7] C. Chow, B. Urquhart, M. Lave, A. Dominguez, J. Kleissl, J. Shields, and B. Washom. (2011, November). Intra-hour forecasting with a total sky imager at the UC San Diego energy testbed. *Solar Energy*. [Online]. 5. Available: <http://dx.doi.org/10.1016/j.solener.2011.08.025>
- [8] J. Schoene, J. Kleissl, V. Zheglov, J. Ning, A. Nguyen, and B. Kurtz. (2013, October). Improving economics of solar power through analysis, forecasting, and dynamic system modeling. Enernex Corp., TN. [Online]. Available: <http://tinyurl.com/ob245mz>
- [9] H. Yang, B. Kurtz, D. Nguyen, B. Urquhart, C. Chow, M. Ghonima, and J. Kleissl. (2014, May). Intra-hour forecasting with a total sky imager at the UC San Diego energy testbed. *Solar Energy*. [Online]. 103, pp. 502-524. Available: <http://dx.doi.org/10.1016/j.solener.2014.02.044>
- [10] D. Nguyen, and J. Kleissl. (2014, September). Stereographic methods for cloud base height determination using two sky imagers. *Solar Energy*. [Online]. 107, pp. 495-509. Available: <http://dx.doi.org/10.1016/j.solener.2014.05.005>
- [11] M. S. Ghonima, B. Urquhart, C. W. Chow, J. E. Shields, A. Cazorla and J. Kleissl (2012). A method for cloud detection and opacity classification based on ground based sky imagery. *Atmospheric Measurement Techniques*. [Online]. 5, pp. 2881-2892. Available: <http://dx.doi.org/10.5194/amt-5-2881-2012>
- [12] M. Lave, and J. Kleissl (2012, August). High-frequency irradiance fluctuations and geographic smoothing. *Solar Energy*. [Online]. 8, pp. 2190-2199. Available: <http://dx.doi.org/10.1016/j.solener.2011.06.031>
- [13] D. Nguyen. (2014, July). Demonstration of cloud overlay on feeder a on Dec 14th 2012. [Online]. Available: <http://solar.ucsd.edu/nguyen/cloudOnFallbrookFeeder520.mp4>
- [14] Video of sky condition on December 18<sup>th</sup> 2014. [Online]. Available: <http://1drv.ms/1HT0euU>
- [15] B. Urquhart, B. Kurtz, E. Dahlin, M. Ghonima, J. Shields, and J. Kleissl (2014). Development of a sky imaging system for short-term solar power forecasting. *Atmospheric Measurement Techniques*. [Online]. 7, pp. 4859-4907. Available: <http://dx.doi.org/10.5194/amt-7-4859-2014>
- [16] R.C. Dugan, T.E. McDermott. (2011 July). An open source platform for collaborating on smart grid research. Presented at the Power and Energy Society General Meeting, 2011 IEEE. [Online]. Available: <http://dx.doi.org/10.1109/PES.2011.6039829>
- [17] <sup>1</sup> Smith, J., Alternatives to the 15% Rule Modeling and Hosting Capacity Analysis of 16 Feeders, Technical Update to the California Solar Initiative RD&D program, EPRI, Palo Alto, CA: 2015. 3002005812. Available online at [http://www.calsolarresearch.org/images/stories/documents/Sol3\\_funded\\_proj\\_docs/EPRI/Modeling-Analysis-16-Feeders\\_3002005812.pdf](http://www.calsolarresearch.org/images/stories/documents/Sol3_funded_proj_docs/EPRI/Modeling-Analysis-16-Feeders_3002005812.pdf).